Coemergence of the Amphipathic Helix on Ameloblastin With Mammalian Prismatic Enamel

Jingtan Su, Rucha Arun Bapat, Gayathri Visakan, and Janet Moradian-Oldak *

Center for Craniofacial Molecular Biology, Herman Ostrow School of Dentistry, University of Southern California, Los Angeles 90033, CA, USA

***Corresponding author:** E-mail: joldak@usc.edu.

Associate editor: Julian Echave

Abstract

To investigate correlation between the ameloblastin (Ambn) amino acid sequence and the emergence of prismatic enamel, a notable event in the evolution of ectodermal hard tissues, we analyzed Ambn sequences of 53 species for which enamel microstructures have been previously reported. We found that a potential amphipathic helix (AH) within the sequence encoded by Exon 5 of *Ambn* appeared in species with prismatic enamel, with a few exceptions. We studied this correlation by investigating synthetic peptides from different species. A blue shift in fluorescence spectroscopy suggested that the peptides derived from mammalian Ambn interacted with liposomes. A downward shift at 222 nm in circular dichroism spectroscopy of the peptides in the presence of liposomes suggested that the peptides of mammals with prismatic enamel underwent a transition from disordered to helical structure. The peptides of species without prismatic enamel did not show similar secondary structural changes in the presence of liposomes. Peptides of mammals with prismatic enamel caused liposome leakage and inhibited LS8 and ALC cell spreading regulated by full-length Ambn. RT-PCR showed that AH is involved in Ambn's regulation of cell polarization genes: *Vangl2*, *Vangl1*, *Prickle1*, *ROCK1*, *ROCK2*, and *Par3*. Our comprehensive sequence analysis clearly demonstrates that AH motif is closely related to the emergence of enamel prismatic structure, providing insight into the evolution of complex enamel microstructure. We speculate that the AH motif evolved in mammals to interact with cell membrane, triggering signaling pathways required for specific changes in cell morphology associated with the formation of enamel prismatic structure.

Key words: **prismatic enamel, ameloblastin, amphipathic helix, enamel evolution, ameloblasts.**

Introduction

Enamel, the hardest mineralized tissue found in vertebrates, caps the teeth of almost all sarcopterygians (lobe-finned bony fishes and tetrapods) as well as the scales and dermal bones of many extinct lobe-fins (Smith 1978; Satchell et al. 2000; Sire et al. 2009; Qu et al. 2015; Berkovitz and Shellis 2017). Its mechanical properties enable teeth to overcome the mechanical resistance of chewing forces (Berkovitz and Shellis 2017). Mature enamel is composed of hydroxyapatite (HAP) crystallites with an architecture that is hierarchically organized, ranging from nanoscale apatite crystals to microscale enamel prisms (rods) (Cui and Ge 2007). Most mammals have prismatic enamel (Boyde 1997; Wood et al. 1999), except a few species that are toothless, enamelless, or have prismless enamel (Davit-Béal et al. 2009; Loch et al. 2013). In prismatic enamel, the HAP crystallites are grouped in parallel bundles (rods or prisms) bounded by interprismatic crystallites (interrods) oriented at a sharp angle to those in the rods (fig. 1). This prism decussation helps in resisting the increasing tendency toward fracture as chewing loads increase and thus contributes to mammalian dietary adaptations (Spears et al. 1993; Rensberger 1997; Tabuce et al. 2017). Most nonmammalian vertebrates, including reptiles except for one extant reptile *Uromastyx maliensis* (Diekwisch 2020), have only prismless enamel (Sander 2000), that is, with HAP crystallites oriented fairly uniformly perpendicular to the enamel surface (Berkovitz and Shellis 2017). Since its origin from the dermal skeleton (Qu et al. 2015), enamel has undergone multiple transitions in its composition and architecture during its evolution (Berkovitz and Shellis 2017). One major architectural transition is from prismless (aprismatic) enamel in reptiles to prismatic enamel in mammals (Sander 1997; Wood et al. 1999). Prismatic enamel is considered a mammalian synapomorphy (Sander 1997; Wood et al. 1999). Fossil evidence suggests that the evolution of prismatic enamel was coincident with that of Tomes' processes of ameloblasts cells, cytoplasmic extensions appearing at the secretoray end of the enamel forming cells during the early stage of enamel formation (amelogenesis) (Lester and Von Koenigswald 1989; Wood et al. 1999).

Formation of tooth enamel mineral occurs in the extracellular matrix (ECM) between secretory ameloblast cells and underlying dentin (Lacruz et al. 2012). This ECM

Article

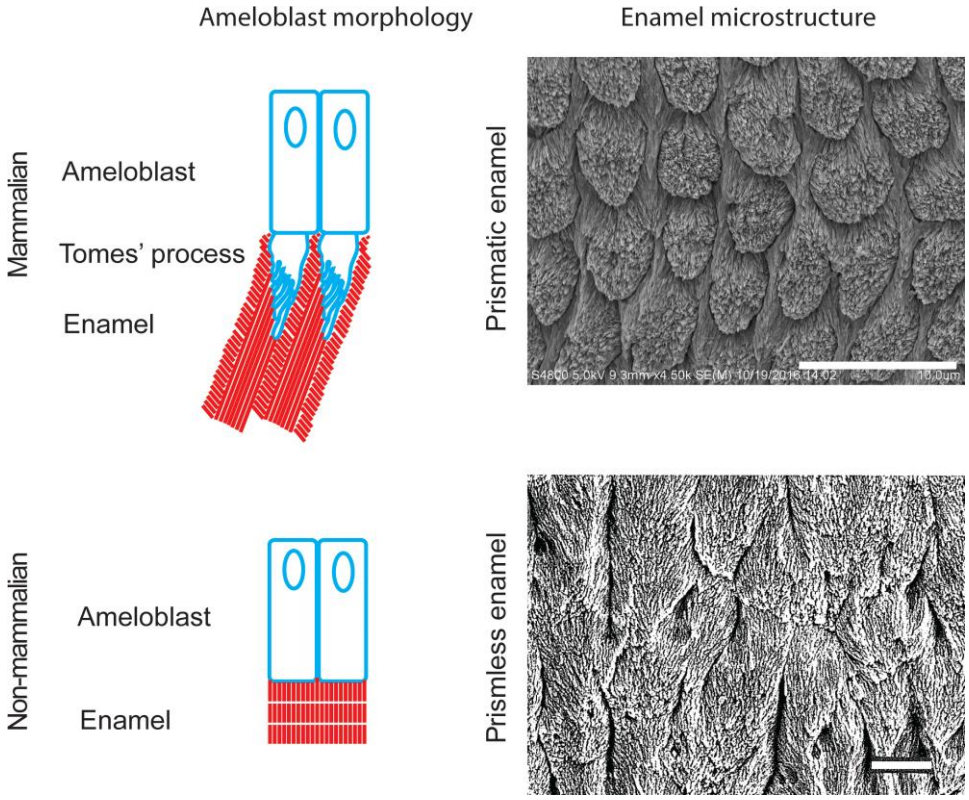

Fig. 1. Schematic images of typical ameloblast morphologies at their secretory stage and SEM of enamel microstructure. Schematic images of ameloblasts were adapted from Line and Novaes (2005); SEM image of human prismatic enamel (courtesy of Dr Changyu Shao), SEM image of reptile prismless enamel was adapted with permission from Sander (1999). Scale bar = 10 μm.

consists of a distinct set of proteins that belong to the family of secretory calcium-binding proteins (SCPPs) and evolved from a common ancestral gene (Sire et al 2007). The main enamel matrix proteins include amelogenin (Amel), ameloblastin (Ambn), enamelin (Enam), and amelotin (Amtn) (Kawasaki and Weiss 2008; Moradian-Oldak 2012). They assemble to create a functional three-dimensional (3D) ECM that serves to control the formation of enamel apatite crystals and are eventually degraded and replaced by the mineral (Fincham et al. 1995; Du et al. 2005; Fang et al. 2011; Wald et al. 2017). Mutations, deletions or misexpressions of *Ambn*, *Amel*, *Enam*, and/or *Amtn* genes cause disturbances in enamel formation affecting HAP crystallite initiation, growth, and organization (Paine et al. 2003; Ozdemir et al. 2005; Jin et al. 2009; Lu et al. 2011; Lacruz et al. 2012; Hu et al. 2014; 2007; Poulter et al. 2014; Smith et al. 2016; Wald et al. 2017). In addition to enamel matrix proteins, mutations in genes related to ameloblast cell attachment apparatus also led to enamel malformation, suggesting their possible function in controlling mineral initiation and elongation during the early stages of amelogenesis (Simmer et al. 2021).

Ambn, the second most abundant enamel matrix protein, is tooth-specific (Krebsbach et al. 1996). DNA sequences of *Ambn* have been reported in the coelacanth, which has enamel, and the spotted gar, which has ganoine, indicating that Ambn appeared during early vertebrate evolution, at least in the last common ancestor of ray-finned fishes (actinopterygians) and lobe-finned fishes (sarcopterygians) 450 Ma (Kawasaki and Amemiya 2014; Braasch et al. 2016). Ambn protein is intrinsically disordered and is enriched in proline, glycine, leucine, and glutamine (Wald et al 2017). The amino acid sequence of Ambn contains positions that have been evolutionarily conserved, indicating their important function in enamel formation (Delsuc et al. 2015). These positions correspond to several cleavage sites and hydroxylated, O-glycosylated, and phosphorylated residues. In addition to the above-mentioned conserved residues, Ambn includes domains (or motifs) such as calcium-binding domain (Yamakoshi et al. 2001), and CD63-interaction domain (Iizuka et al. 2011; Delsuc et al 2015) that are partially conserved among species. Cell attachment motifs such as the integrin-binding (Cerny et al. 1996) and heparin-binding motifs (Sonoda et al. 2009), were reported in rodent and are not conserved in mammalian evolution suggesting that these motifs could have a functional role only in rodents. Fibronectin-binding motifs were identified in rat and human Ambn (Beyeler et al. 2010).

Studies based on gain and loss of Ambn function in animal models indicate that Ambn may be involved in cell–matrix adhesion (Fukumoto et al. 2004), the maintenance of the prismatic structure (Mazumder et al. 2016; Wald et al 2017), and the regulation of the mineralization process (Krebsbach et al. 1996; Paine et al 2003; Liang et al 2019). For example, Ambn overexpression in mouse influences the habit of enamel crystallites and the morphology of enamel rods (Paine et al. 2003), which are the basic units of prismatic microstructure. Mutation of the *Ambn* gene in mouse causes loss of polarity in ameloblast cells and

their detachment from the extracellular matrix leading to severe enamel malformation (Wald et al. 2017).

Recently, we reported that mammalian Ambn has a highly conserved amphipathic helix (AH) motif, located within the sequence encoded by Exon 5 (Su et al. 2019a). AH is an α-helix with opposing polar and nonpolar faces oriented along its long axis (Segrest et al. 1994) . AH motifs are involved in multiple cellular functions, such as anchoring peripheral proteins on membranes (Pataki et al. 2018), deforming lipid bilayers (Brady et al. 2015), and sensing membrane curvature (Hatzakis et al. 2009), as well as in signaling pathways (Carman and Dominguez 2018). We also reported that the Exon 5-encoded region of Ambn contributes to promoting polarization of ameloblast cell lines in a 3D cell culture system (Visakan et al. 2022). Furthermore, in a 2D cell culture model we showed that the AH motif within the same sequence encoded by Exon 5 mediates Ambn-cell adhesion (Su et al. 2020).

Considering that the AH appears only in mammalian Ambn and that prismatic enamel is a mammalian synapomorphy, here we hypothesized a novel correlation between the evolutionary emergence of the AH motif and prismatic enamel within mammals. To test this correlation, we performed AH prediction analysis on Ambn sequences from 53 species and associated these sequences with the enamel microstructures reported in the literature. We then experimentally validated the presence of the functional AH motif in 10 of these species by investigating the interactions of species-specific synthetic peptides with large unilamellar vesicles (LUVs), a model for cell membrane, and by investigating the function of these peptides using cell-based assays. We then investigated the potential function of Ambn in upregulating ameloblast cell polarization genes, which may directly or indirectly affect the development of Tomes' processes in ameloblasts and consequently prismatic enamel formation.

Results

Phylogenetic Tree

The Maximum Likelihood (ML) phylogram inferred from 53 full-length Ambn protein sequences under the JTT + GAMMA model is presented in Figure 2. The Ambn sequences studied here represent 44 families distributed across 28 orders (supplementary table S1, Additional file 1, Supplementary Material online) and were aligned by MAFFT, which is one of the most accurate sequence alignment programs (Additional file 2, Supplementary Material online) (Nuin et al. 2006). The phylogenetic tree showed that Ambn contains a strong phylogenetic signal, consistent with a previous report (Delsuc et al. 2015). The phylogenetic tree supports the three bony vertebrate clades: Actinopterygii, Sarcopterygii, and Tetrapoda; and the major Tetrapoda clades: Amphibia, Reptilia (birds not included), and Mammalia. Within Mammalia, monotremes diverged from the living therians before marsupials and placentals separated from each other. Within the placentals, Xenarthrans and Afrotherians diverged from Boreoeutherians before the latter divided into Euarchontoglires and Laurasiatherians (supplementary fig. S1, Supplementary Material online).

An AH in Ambn is Associated With Prismatic Enamel

The Ambn sequences were screened for the presence of the AH motif using Heliquest and were compared with the enamel microstructures, that is, prismatic or prismless. The predicted AH motif is composed of 18 residues ("RLGFGKALNSLWLHGLLP" in mouse) that form a helix with a hydrophilic face and a hydrophobic one (Su et al. 2019a). Interestingly, the predicted AH sequences frequently coemerge with the prismatic enamel microstructures in mammals (fig. 2). Out of 42 studied mammals, 33 have a predicted AH motif within the protein sequence encoded by Exon 5 of *Ambn*. In these 33 mammals with a predicted AH motif, 26 have prismatic enamel and we can infer those 4 others might also have prismatic enamel according to the reported enamel microstructure of other species in the same genus. The only species in the group with a predicted AH motif but confirmed not to have prismatic enamel are whales (*Balaenoptera acutorostrata scammoni*, *Metapenaeus monoceros*, and *Physeter macrocephalus*); we discuss these species further in the next section. A predicted AH motif, however, is not found in mammals without prismatic enamel (except the whales as mentioned above), reptiles, amphibians, sarcopterygians (excluding tetrapods), or actinopterygians. Notably, the Ambn of *Ornithorhynchus anatinus*, a survivor of an early branch from the mammalian tree (Messer et al. 1998), contains the predicted AH motif, even though only part of its enamel is prismatic and regular prisms are not the primary feature of its enamel structure (Lester and Boyde 1986). *O. anatinus* has prismatic enamel only in juvenile stages; adults of the species lack enamel (Lester et al. 1987). This might be because *O. anatinus* has apparently nonfunctional MMP20 and Amtn (Kawasaki and Suzuki 2011; Gasse et al. 2015) but apparently functional Ambn and Enam (Warren et al. 2008). The occurrence of prismatic enamel and Ambn in *O. anatinus* implies the role of Ambn in the development of prismatic enamel. Ambn protein from two mammalian species without enamel, namely *Dasypus novemcinctus* and *Orycteropus afer afer* (Davit-Béal et al. 2009), lost the ability to form an AH motif because the aspartic acid residue, highlighted in red (fig. 2), reduced the net charge from +2 to +1. This observation supports that there is a close correlation between the conserved AH motif and prismatic enamel.

Exceptions to the Correlation Between AH and Prismatic Enamel

There are a few exceptions to the abovementioned correlation. Two eutherians (*Elephantulus edwardii* and *Fukomys damarensis*) and four marsupials (*Monodelphis domestica*, *Sarcophilus harrisii*, *Dromiciops gliroides*, and *Phascolarctos cinereus*) have prismatic enamel, although

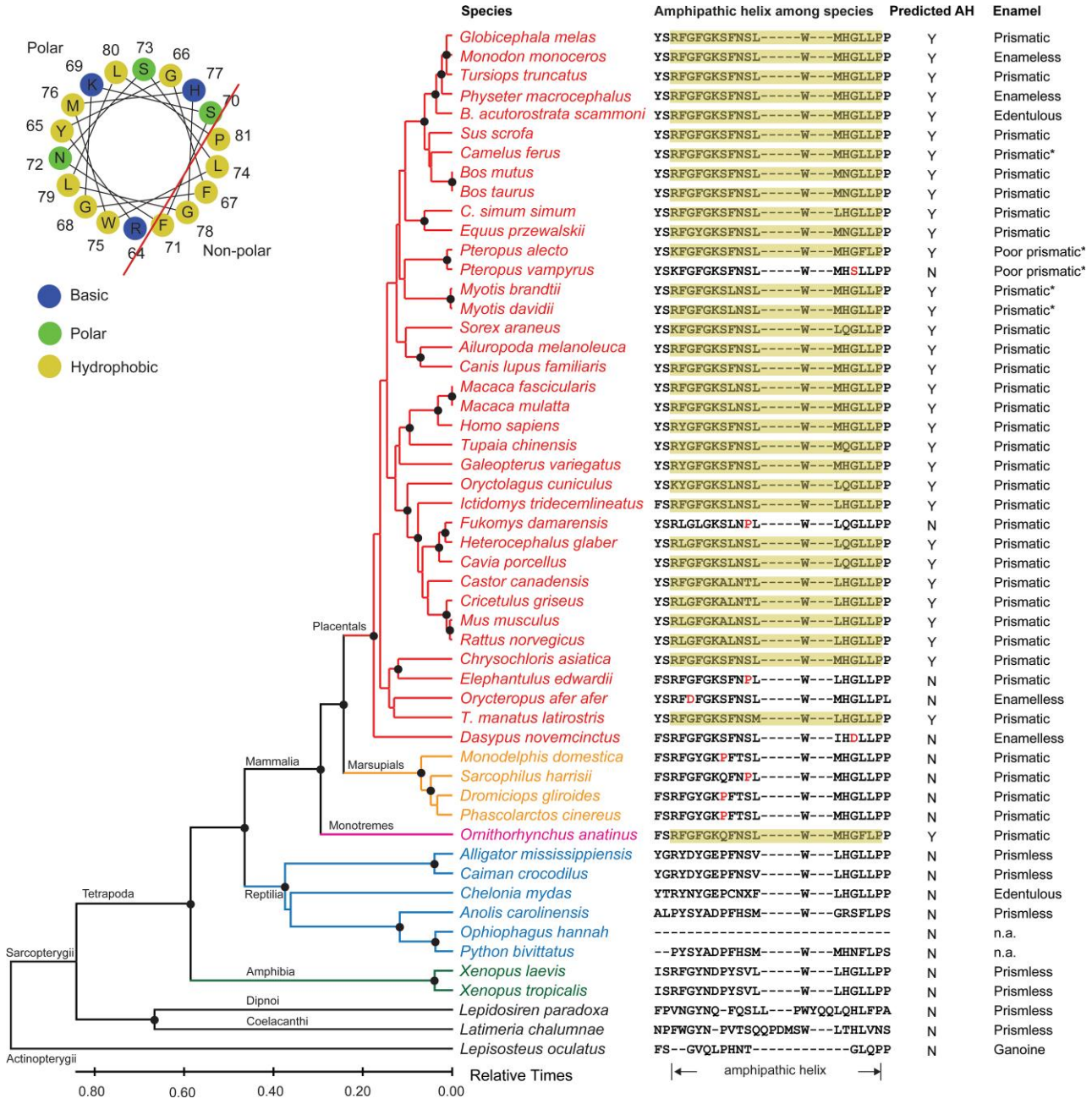

Fig. 2. Evolutionary correlation between predicted amphipathic helix (AH) with enamel prismatic and nonprismatic structures. The helical wheel shows the typical AH of human Ambn, with a large polar face and a small nonpolar face oriented along its long axis. Maximum likelihood tree (JTT + GAMMA model) was constructed using Ambn protein sequences from 53 species. Spotted gar (*Lepisosteus oculatus*) was used as outgroup. Nodes with more than 70% bootstrap support are indicated with dots. The phylogenetic relationships among placentals are shown in details in supplementary fig. S1, Supplementary Material online. The predicted AH in Ambn sequences are highlighted. In predicted AH column, Y: Ambn has a predicted AH motif in Exon 5; N: Ambn has no predicted AH motif in Exon 5. In Enamel column, * indicates the enamel microstructure was inferred from reported enamel microstructure of species in the same genus.

theoretically their AH formation may be blocked by a proline residue in the middle of the sequence. In order to show whether there is an AH motif in Ambn in these species, we investigated its presence experimentally using biophysical and cell-based assays, on which we report below.

Another notable exception is related to the three whale species noted above: *B. acutorostrata scammoni* is edentulous, and *M. monoceros* and *P. macrocephalus* have teeth which are enamelless. These three whales have predicted AH motifs and the amino acid sequences of the AH motifs are the same as those of some mammals with prismatic

Table 1. Summary of the Relationship Between Predicted AH and Enamel Microstructure in the 53 Species Studied.

Group	Predicted AH	Factors destroying AH	Enamel microstructure	Distribution
I	Y	n.a.	Prismatic	26 placentals
			Prismatic[a]	4 placentals
II	N	Pro in the middle	Prismatic	4 marsupials
				2 placentals
III	N	Ser disroying hydrophobic face	Poor prismatic[a]	1 placental
IV	N	Asp reducing positive charges	Enamelless	2 placentals
V	N	Multiple factors including negatively or zero net charge, and middle Pro.	Edentulous, enamelless, prismless	*Lepisosteus oculatus*
				Latimeria chalumnae
				Lepidosiren paradoxa
				2 Amphibians
				4 reptiles
VI	Y	n.a.	Edentulous, enamelless	3 whales

In Predicted AH column, Y indicates there is a predicted AH, N indicates there is no predicted AH. Group VI is found only in whales.
[a]Enamel microstructure was inferred from the reports of other species in the same genus. *Notes*: 1. In Group I, the enamel prismatic microstructure of 26 plancentals are well-supported by documents, and the enamel prismatic microstructure of four species are inferred from that of other species in the same genus; 2: *Python bivittatus* and *Ophiophagus hannah* is not included in the statistics since there is no report about their enamel microstrucure.

enamel, such as *Globicephala melas*, *Tursiops truncates*, and *Sus scrofa*.

Grouping of the Species Based on the Bioinformatic Outcomes

The bioinformatic outcomes revealing the presence or absence of predicted AH motifs in the Ambn sequence from different species were used as a basis to create six groups (table 1). Group I: Ambn sequences have predicted AH and the species have prismatic enamel; Group II: The species have prismatic enamel but Ambn sequences have no predicted AH because of the presence of Pro; Group III: The species might have poor prismatic enamel but Ambn sequence has no predicted AH because of the presence of Ser; Group IV: The species have nonprismatic enamel and Ambn sequences have no predicted AH because of the presence of Asp; Group V: The species have nonprismatic enamel, and because of multiple factors that disturb AH folding, Ambn sequences have no predicted AH; Group VI: Ambn sequences have predicted AH but the species are edentulous or enamelless.

Out of a total of 51 species (excluding *Ophiophagus hannah* and *Python bivittatus*), 37 species (26 from Group I, 2 from Group IV, and 9 from Group V) support the correlation between the presence of predicted AH on Ambn sequence and prismatic enamel. Four species from Group I may support this correlation but there is some uncertainty six species (Group II) do not support because of the presence of Pro which hinders prediction of AH, one species from Group III may or may not support it, and three species (Group VI, the three whales) are not relevant because they are edentulous or enamelless. Group I contain 30 placentals with AH that have or should have prismatic enamel. Group II contains four marsupials and two placentals with prismatic enamel, but their potential AH may be disrupted by a middle proline residue. Group III consists of only one placental mammal that may have poor prismatic enamel, and its AH hydrophobic face may be disrupted by a serine residue. Group IV contains two enamelless placentals that have their potential AH disrupted by an aspartic acid residue. Group V contains nine species without prismatic enamel that have no predicted AH. Group VI contains three whales with predicted AH that have no enamel.

Design and Characteristics of Ambn-Derived Synthetic Peptides for Biophysical and Cell-based Assays

We designed peptides derived from AH sequences of 10 selected species, which we used for our biophysical and cell-based experiments (table 2). These peptides are from Groups I to V, and include a selection of six placentals, one metatherian, one prototherian, one reptile and one amphibian. These peptides were each at the N-terminus of the sequence encoded by Exon 5 of Ambn. Two extra amino acids were added at the N-terminus to help helical folding (Scholtz and Baldwin 1992). The length of each peptide was 20 residues. Each peptide may represent more than just the species listed in table 2, because different species may have the same amino acid sequence in the selected region.

Peptides from *Homo sapiens* (Eutheria), *Mus musculus* (Eutheria), and *O. anatinus* (Prototheria) are in Group I (table 2). These species have prismatic enamel, and as predicted by Heliquest have a predicted AH. The AH sequence of *H. sapiens* is also found in *Gorilla gorilla gorilla*, *Pongo abelii*, *Pan paniscus*, *Pan troglodytes*, *Crocuta crocuta*, and *Galeopterus variegatus*. *G. gorilla gorilla*, *P. abelii*, *P. paniscus*, and *P. troglodytes* are all in the same order as *H. sapiens*, that is, primates, which have prismatic enamel (Boyde and Martin 1984). *C. crocuta* also has prismatic enamel (Rensberger and Wang 2005). There is no report on the enamel microstructure of *G. variegatus*. The AH sequence of *M. musculus* is also found in *Arvicanthis niloticus*, *Grammomys surdaster*, *Mastomys coucha*, *Mesocricetus auratus*, *Mus caroli*, *Mus pahari*, *Rattus norvegicus*, and *Rattus rattus*. All these species are rodents with prismatic enamel (von Koenigswald 1985; Alloing-Séguier et al.

Table 2. Synthetic Peptides Derived From AH Sequence Selected From Different Species With Prismatic and Nonprismatic Structures.

Classification	Species	Sequences of the peptides	Predicted AH	Group
Mammal, Theria, Eutheria	***Homo sapiens***	^{62}YSRYGFGKSFNSLWMHGLLP^{81}	**Y**	**I**
	Mus musculus	^{67}YSRLGFGKALNSLWLHGLLP^{86}	**Y**	**I**
	Elephantulus edwardii	^{62}FSRFGFGKSFNPLWLHGLLP^{81}	**N**	**II**
	Pteropus vampyrus	^{52}YSKFGFGKSFNSLWMHSLLP^{71}	**N**	**III**
	Dasypus novemcinctus	^{52}FSRFGFGKSFNSLWIHDLLP^{71}	**N**	**IV**
	Orycteropus afer afer	^{62}YSRFDFGKSFNSLWMHGLLP^{81}	**N**	**IV**
Mammal, Theria, Metatheria	***Monodelphis domestica***	^{55}FSRFGYGKPFTSLWMHGLLP^{74}	**N**	**II**
Mammal, Prototheria	***Ornithorhynchus anatinus***	^{149}FSRFGFGKQFNSLWMHGFLP^{168}	**Y**	**I**
Reptile	***Alligator mississippiensis***	^{51}YGRYDYGEPFNSVWLHGLLP^{70}	**N**	**V**
Amphibian	***Xenopus laevis***	^{52}ISRFGYNDPYSVLWLHGLLP^{70}	**N**	**V**

In Predicted AH column, Y indicates the sequence of the peptide has a predicted amphipathic helix; Nindicates the sequence of the peptide has no predicted amphipathic helix. Residues which may impede the formation of an amphipathic helix are highlighted in red. In Group column, the peptides were grouped according to table 1.

2019). The AH sequence of *O. anatinus* is not found in any other species.

Peptides from *E. edwardii* (Eutheria) and *M. domestica* (Metatheria) are in Group II, which has prismatic enamel but no predicted AH. This peptide sequence of *E. edwardii* is not found in any other species. The peptide sequence of *M. domestica* is also found in *P. cinereus*, another marsupial with prismatic enamel (Young et al. 1987).

Peptides from *Pteropus vampyrus* are in Group III and have no predicted AH due the hydrophobic face being disrupted by a polar serine residue (supplementary fig. S2, Supplementary Material online). We were unable to find an SEM image of *P. vampyrus* enamel in the literature. However, an SEM image of the enamel of *Pteropus scapulatus*, which is in the same genus, revealed very thin enamel, with just one to two rows of prisms with largely rounded outlines, and an extensive prism-free outer zone of parallel crystallite groups (Lester and Hand 1986). Due to limited access to enamel samples from *P. vampyrus*, we were unable to confirm our conjecture that *P. vampyrus* might be poorly prismatic or even prismless. The peptide sequence of *P. vampyrus* is also found in *P. giganteus*, another bat in the same genus, whose enamel microstructure has not been reported. *P. vampyrus* was analyzed in this study because it is a species with a polar serine residue which may disrupt the hydrophobic face of the potential AH motif.

Peptides from *D. novemcinctus* and *O. afer afer* are in Group IV, which are enamelless species and have no AH. The presence of an aspartic acid residue reduces the positive charges of the helix and disrupts the formation of AH of both *D. novemcinctus* ($D = 0.44$) and *O. afer afer* ($D = 0.51$) (supplementary table S1, Supplementary Material online). Neither the peptide sequence of *D. novemcinctus* nor the peptide sequence of *O. afer afer* are found in any other species.

Peptides from *Alligator mississippiensis* and *Xenopus laevis* are in Group V, which are prismless and have no AH. *A. mississippiensis* is a reptile. The sequence of *A. mississippiensis* is also found in *Alligator sinensis*, *Caiman crocodilus*, *Crocodylus porosus*, and *Gavialis gangeticus*, respectively from the families Alligatoridae, Crocodylidae, and Gavialidae of the order Crocodylia, which have prismless enamel (Sander 1997, 1999). *X. laevis* is an amphibian, and the peptide sequence of *X. laevis* is also found in *Xenopus tropicalis*, another kind of frog with prismless enamel (Davit-Béal et al. 2007).

Peptides Derived From Mammalian Ambn Interact With LUV

LUV have been demonstrated to be an appropriate model to mimic cell membrane regions involved in epithelial cell–ECM adhesion (Su et al. 2019a). We used intrinsic fluorescence spectroscopy to test the electrostatic attraction of the peptides to LUV by investigating the blue shift of the peptides upon the addition of LUV (fig. 3). The peptides in Groups I–IV showed significant blue shift with the addition of LUV (fig. 3 *A*–*H*), indicating that the added LUV interacted with the peptides and made the local environments of the tryptophan residues more hydrophobic. Considering that the liposome used in this assay was negatively charged, and that the peptides were positively charged, it is likely that the charged peptides of mammals were attracted electrostatically to the LUV surface. In contrast, there was no visible blue shift for the peptides of Group V, indicating that the added LUV did not come close to the peptides in solution, and suggesting that LUV did not interact with these peptides of reptiles or amphibians (fig. 3*I*, *J*).

Helical Content of Peptides of Mammals With Prismatic Enamel Increases With LUV

We then used circular dichroism (CD) spectroscopy to track helix formation by investigating the secondary structural changes of the peptides upon the addition of LUV. The peptide concentration for CD spectroscopy was 100 μM, 10 times that used for fluorescence spectroscopy. This high peptide concentration led to slight aggregation in the CD cell for the peptides from *H. sapiens*, *O. anatinus*, *E. edwardii*, and *O. afer afer*; and moderate aggregation in the CD cell for the peptides from *M. domestica*, *P. vampyrus*, and *D. novemcinctus*. All these aggregate peptides showed a maximum peak between 220 and 230 nm in the CD spectrum (fig. 4).

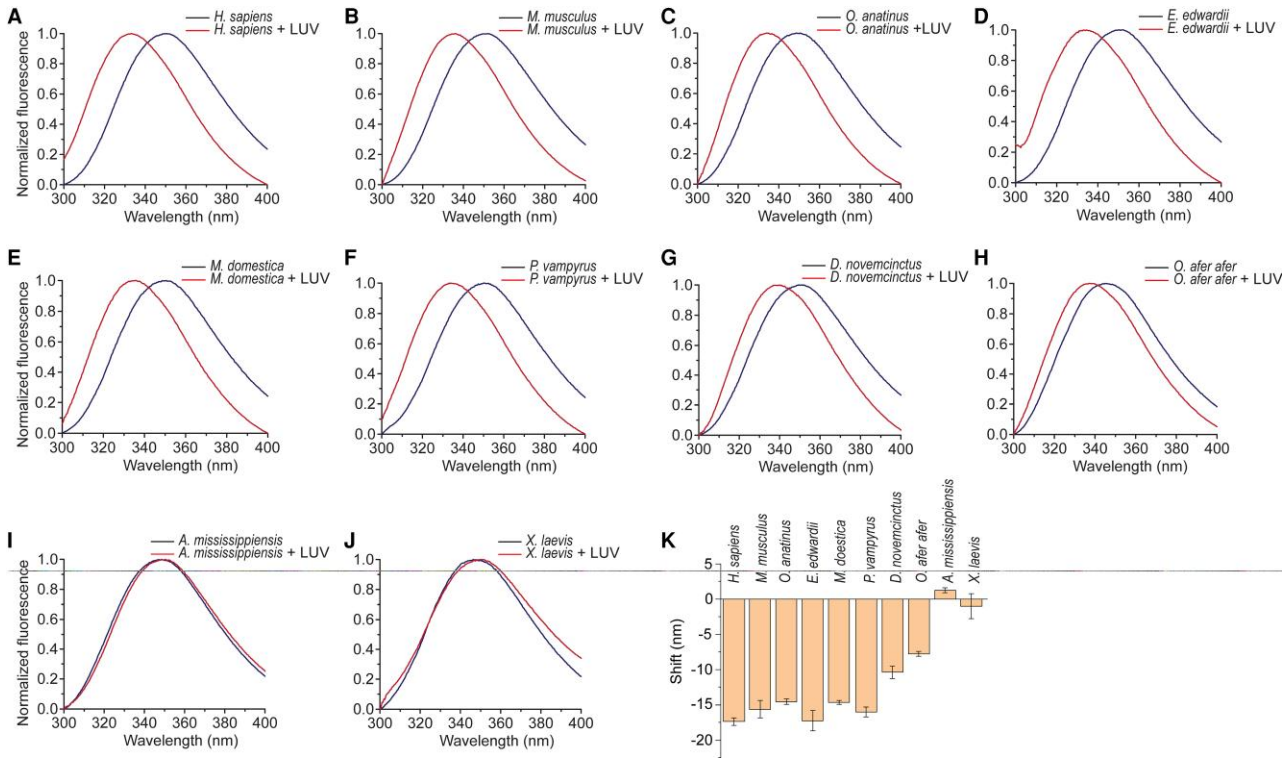

Fig. 3. Intrinsic fluorescence spectroscopy of 10 μM Ambn-derived peptides titrated with 300 μM LUV. The peptides of all mammals including *Homo sapiens* (*A*), *Mus musculus* (*B*), *Ornithorhynchus anatinus* (*C*), *Elephantulus edwardii* (*D*), *Monodelphis domestica* (*E*), *Pteropus vampyrus* (*F*), *Dasypus novemcinctus* (*G*), *Orycteropus afer afer* (*H*) showed significant blue shift when LUV were added. In contrast, the peptides of reptiles such as *Alligator mississippiensis* (*I*) and amphibians such as *Xenopus laevis* (*J*) did not show a blue shift. The blue shifts are summarized in (*K*).

Before adding LUV, all the peptides except that of *O. afer afer* showed a minimum peak between 200 and 210 nm, and a value close to zero or below zero at around 195 nm, suggesting that these peptides lacked well-defined structures at pH 7.4. This result is consistent with the random coil secondary structure predicted with high confidence by I-TASSER (supplementary fig. S3, Supplementary Material online). Lacking well-defined structures might be a reason why the peptides aggregate at 100 μM. *O. afer afer* showed a minimum peak at around 218 nm and a positive value at around 195 nm, suggesting that *O. afer afer* has preformed secondary structures.

In Group I, the behavior of the peptide from *M. musculus* was consistent with our previous report (Su et al. 2019a), that is, there was a random coil-to-helix conformational transition (fig. 4*B*), which is a typical behavior of the AH motif (Seelig 2004). The CD spectra of the peptides from *H. sapiens* and *O. anatinus* were affected by peptide aggregation. However, minimum peaks appeared at around 222 nm and the CD value at 195 nm increased (fig. 4*A* and *C*), suggesting that the two peptides gained some well-defined structures when LUV were added, and this secondary structure was predominantly helical. A random coil-to-α-helix conformational transition also happened to the peptides from *H. sapiens* and *O. anatinus*.

In Group II, peptide aggregation affected the conformational changes detected by CD. With the addition of LUV, the CD value decreased at around 222 nm (fig. 4*D* and *F*), suggesting that the peptides from *E. edwardii* and *M. domestica* underwent detectable secondary conformational changes.

In Groups III and IV, the behavior of peptides from *P. vampyrus*, *D. novemcinctus*, and *O. afer afer* was similar to that of the peptide from *E. edwardii* (fig. 4*F*–*H*). Peptides from *P. vampyrus* and *D. novemcinctus* showed a slight decrease at around 222 nm, suggesting an increase of secondary structural content, but the results did not indicate an increase of helical content because there was no minimum peak at around 222 nm. *O. afer afer* showed slight changes, but the increase was at around 200 nm, implying that a smaller amount of well-defined structure was forming.

In Group V, peptides from *A. mississippiensis* and *X. laevis* did not show significant CD value changes (fig. 4*I* and *J*), suggesting that these two peptides did not undergo any conformational changes. A slight decrease between 195 and 210 nm was observed for the peptide from *X. laevis* but may have been the result of background noise and does not suggest any structural change.

Peptides of Mammals With Prismatic Enamel Anchor to Lipid Membrane

A membrane leakage assay was used to test for membrane insertion, a typical behavior which is important for the

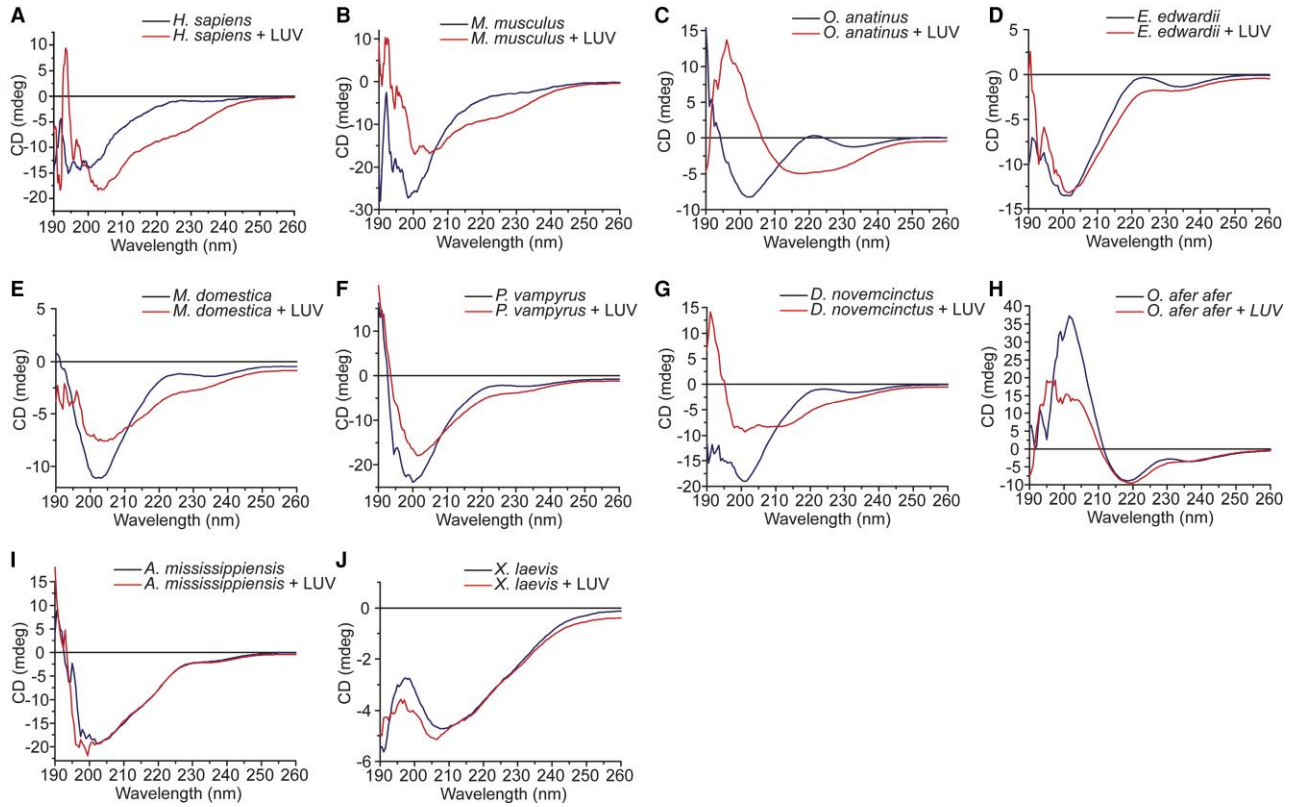

Fig. 4. Circular dichroism spectroscopy of 100 μM Ambn-derived peptides titrated with 300 μM LUV. *Homo sapiens* (*A*), *Mus musculus* (*B*), *Ornithorhynchus anatinus* (*C*), *Elephantulus edwardii* (*D*), *Monodelphis domestica* (*E*), *Pteropus vampyrus* (*F*), *Dasypus novemcinctus* (*G*) showed a downward peak at 222 nm when LUV were added. In contrast, *Orycteropus afer afer* (*H*), *Alligator mississippiensis* (*I*) and *Xenopus laevis* (*J*) did not show a detectable downward trend at 222 nm when LUV were added.

function of the AH motif (Giménez-Andrés et al. 2018). If a peptide causes leakage of a lipid membrane in this test, it can be inferred that the peptide forms a functional AH even if its helical content could not be detected by CD.

In Groups I and II, the fluorescence signals increased significantly (fig. 5*A*–*C*), suggesting that all these peptides caused leakage of the lipid membrane of liposomes to some extent. Consistent with our previous report (Su et al. 2019a), the peptide from *M. musculus* always caused a large amount of liposome leakage. The peptide from *H. sapiens* caused liposome leakage, while not always as efficiently as that of *M. musculus*. In some cases, the peptide from *H. sapiens* caused moderate leakage, like *O. anatinus*. The variability between different replicates of this assay might be due to the different solubility of the peptide from *H. sapiens*. Peptides from *O. anatinus* always caused moderate leakage. Despite our *in silico* analysis suggesting that *E. edwardii* and *M. domestica* do not have a predicted AH, these peptides always caused moderate leakage as well. We therefore speculate that, despite their potentially disruptive proline residues, these two peptides formed functional amphipathic helices which could be inserted into the liposome lipid membrane.

In Groups III and IV, the fluorescence signals barely increased, suggesting that peptides from *P. vampyrus*, *D. novemcinctus*, and *O. afer afer* did not cause the leakage of the liposomes (fig. 5*D* and *E*). From this it can be inferred that these peptides did not insert into the lipid membrane, even if they interacted with the liposomes as shown by fluorescence spectra and underwent slight structural changes as shown by CD.

In Group V, the fluorescence signals did not increase (fig. 5*F*), suggesting that peptides from *A. mississippiensis* and *X. laevis* did not cause leakage of the liposomes at all. This is consistent with the fluorescence spectroscopy which showed that they were not adsorbed by the liposomes, and CD which showed that they did not undergo conformational changes with the addition of liposomes.

Peptides of Mammals With Prismatic Enamel Inhibit Cell Spreading on Ambn-Coated Plates

Cell spreading assays were conducted to test the biological functions of the AH motif. Two ameloblast-like cells, LS8 and ALC, which represent early and later stages of ameloblast cells, respectively (Sarkar et al. 2014), were mixed with the AH-derived peptides and then cultured on Ambn-coated plates. The relative numbers of spreading cells were then calculated by counting both the spreading cells and nonspreading cells. Peptide AB2C, which is located at the C-terminal of the sequence encoded by Exon 5, adjacent to the AH motif of *M. musculus Ambn*,

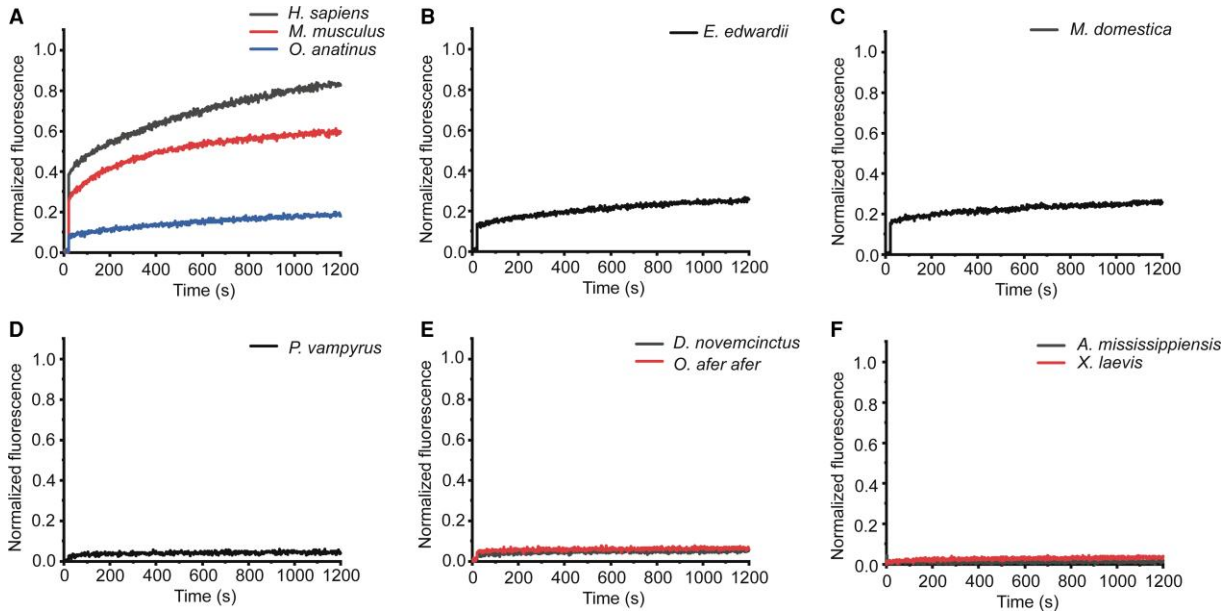

Fig. 5. Membrane leakage assay with 1 μM Ambn-derived peptides. The peptides of *Homo sapiens*, *Mus musculus*, *Ornithorhynchus anatinus*, *Elephantulus edwardii*, and *Monodelphis domestica* resulted in a significant increase in fluorescence signal (*A*–*C*), suggesting that these peptides caused significant membrane leakage. In contrast, the peptides of *Pteropus vampyrus*, *Dasypus novemcinctus*, and *Orycteropus afer afer* showed a slight increase in fluorescence signal (*D* and *E*), suggesting that these peptides caused minor membrane leakage. The peptides from *Alligator mississippiensis* and *Xenopus laevis* showed no increase (*F*), suggesting that these peptides did not cause leakage.

does not have an AH motif and therefore was used as negative control in addition to PBS alone. In Group I, the relative numbers of spreading cells with the peptide from *M. musculus* were 0.04 ± 0.04 for LS8 (fig. 6*A*) and 0.67 ± 0.19 for ALC (fig. 6*B*), both of which were lower than the AB2C and PBS controls, suggesting that the peptide from *M. musculus* inhibited the spreading of both types of cells. The relative numbers of spreading cells with the peptide from *H. sapiens* were 0.30 ± 0.03 for LS8 and 0.70 ± 0.03 for ALC, and with the peptide from *O. anatinus was* 0.33 ± 0.03 for LS8 and 0.69 ± 0.08 for ALC. All these numbers were lower than those of controls, suggesting that the peptides in Group I inhibited cell spreading by competing with full-length recombinant mouse Ambn coated on the plates.

In Group II, the relative numbers of spreading cells with the peptide from *E. edwardii* were 0.10 ± 0.05 for LS8 and 0.59 ± 0.04 for ALC, and with the peptide from *M. domestica* were 0.46 ± 0.07 for LS8 and 0.75 ± 0.02 for ALC. These values were lower than those of controls, suggesting that the peptides from *E. edwardii* and *M. domestica* inhibited cell spreading by competing with full-length mouse Ambn coated on the plate, *that is*, the two peptides were functional in inhibiting cell spreading despite the proline in a potentially disruptive position.

In Groups III, IV, and V, the relative numbers of spreading cells were not significantly different from those of controls, suggesting that the peptides from *P. vampyrus*, *D. novemcinctus*, *O. afer afer*, *A. mississippiensis*, and *X. laevis* did not inhibit spreading of LS8 and ALC on Ambn-coated plates.

Ambn Increases Expression of Genes Related to Cell Polarization

It has been reported that prismatic structure is closely related to Tomes' processes, which are present at the apical or secretory end of mammalian ameloblast cells (Moss-Salentijn et al. 1997). Thus, we examined whether Ambn can regulate the expression of genes which are involved in ameloblast polarity and Tomes' process development (Nishikawa and Kawamoto 2015; Otsu and Harada 2016) (fig. 7). After treating LS8 cells with Ambn for 4 h, the mRNA level of *Vangl2*, a planar cell polarity gene which is abundantly expressed at Tomes' processes, was increased by 2.8 times compared to the untreated group. mRNA levels of *Vangl1* and *Prickle1*, two planar cell polarity genes which are abundant at the distal junctional area of secretory ameloblasts forming the inner layer of enamel (Nishikawa and Kawamoto 2015), were respectively increased by 3.5 times and 4.1 times after treatment with Ambn. mRNA levels of *ROCK1* and *ROCK2*, two genes in RhoA-ROCK signaling pathway which are involved in actomyosin assembly contraction and/or actin depolymerization (Otsu and Harada 2016), were respectively increased by 6.9 times and 3.7 times. The mRNA level of *Par3*, a gene in Cdc42 signaling pathway which is involved in cell polarization/cell–cell adhesion (Chiba et al. 2020), was increased by 3.8 times. Our recent report that Ambn promotes polarization of ameloblast cell lines further supports that Ambn might be involved in determining enamel microstructure through regulating ameloblast polarity or Tomes' process development (Visakan et al. 2022).

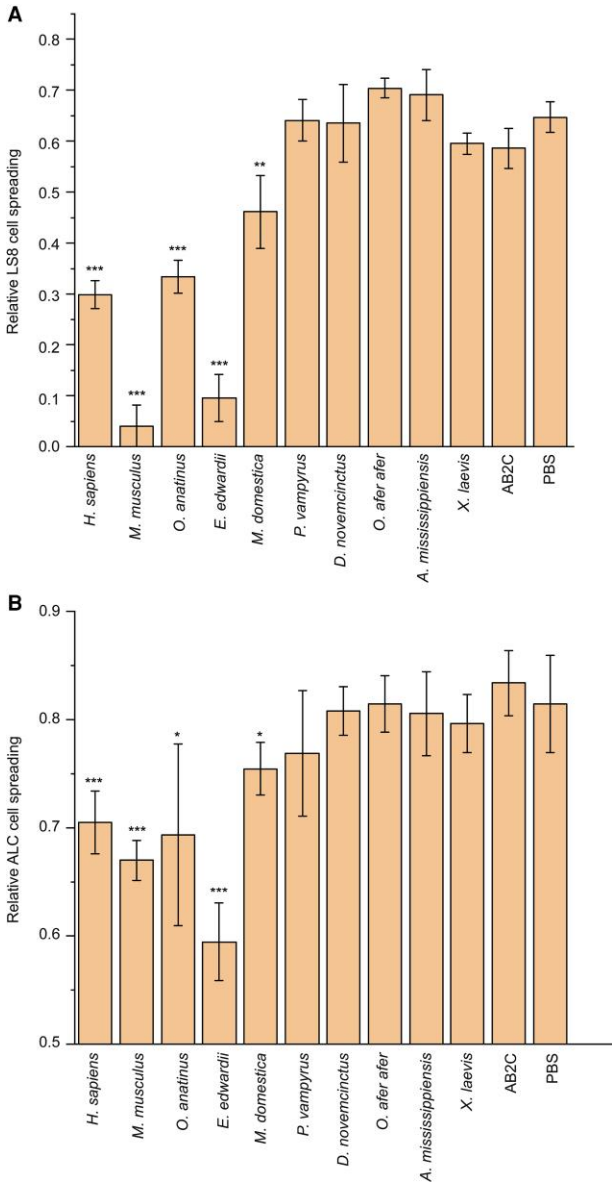

Fig. 6. Cell spreading assay on plates coated with 10 µg/ml recombinant mouse Ambn and 40 µg/ml Ambn-derived peptides. The peptides of *Homo sapiens*, *Mus musculus*, *Ornithorhynchus anatinus*, *Elephantulus edwardii*, and *Monodelphis domestica* inhibited the cell spreading of LS8 cells (*A*) and ALC cells (*B*), while other peptides did not. $^{*}P < 0.05$; $^{**}P < 0.01$; $^{***}P < 0.001$.

To examine the function of the AH motif in regulating ameloblast differentiation and/or cell polarity, expression of *Vangl2* was analyzed in LS8 cells treated with heat denatured Ambn and AmbnΔ5, which were used as negative controls. AmbnΔ5 is the variant missing the entire sequence encoded by Exon 5, and thus without the AH motif. The heat denatured Ambn and AmbnΔ5 groups showed no significant difference from the control without treatment, and *Vangl2* gene expression in the group with full-length Ambn was about twice that of the other groups (fig. 7*B*), suggesting that the AH motif is involved in Ambn's function in ameloblast development and/or cell polarity.

Discussion

Prismatic enamel is vital to mammalian functional adaptation in response to the increased biomechanical stress loaded on teeth (Spears et al. 1993; Rensberger 1997; Sander 1997; Wood et al. 1999) and is a result of the shape and function of the Tomes' processes of the secretory ameloblasts (Nanci and Warshawsky 1984). Ameloblasts secrete enamel SCPPs including Amel, Ambn, Enam, Amtn and Odam, which are all critical for normal enamel development and mineralization (Kawasaki and Weiss 2008). While certain regions in these proteins are highly conserved across all species with enamel, indicating their common functional significance in enamel formation, other regions have distinctive differences between mammals and nonmammals. For example, only 77 out of 1,550 positions in Enam (5%) and 80 out of 447 (18%) positions in Ambn have remained unchanged during the approximately 220 million years of mammalian evolution (Al-Hashimi et al. 2009; Delsuc et al. 2015). Examples of differences in common motifs across various species include the mammalian Amel, which has a longer polyproline tripeptide repeat sequence than nonmammalian Amel (Delgado et al. 2005; Diekwisch et al. 2009). The elongated polyproline tandem repeat is associated with enamel apatite crystal length (Jin et al. 2009). Another example is the structure of nonmammalian Amtn, which differs from mammalian Amtn, with a RGD motif at its C-terminus. Furthermore, Amtn is expressed throughout all stages of amelogenesis in nonmammalian tetrapods, while in rodents its expression is limited to the maturation stage of enamel (Gasse et al. 2015). The above differences between mammalian and nonmammalian enamel matrix proteins have been linked to the evolution of prismatic enamel by many investigators, but the genetic and molecular basis for the emergence of prismatic microstructure has remained unclear.

In the present study we link the evolutionary changes in the AH motif of Ambn sequence to the emergence of prismatic enamel in mammals. Below we provide explanation for the lack of such association in a few exceptional cases noted in our investigation. Among the 53 species we analyzed using bioinformatic methods, we observed that the mammals with predicted AH on Ambn (except the three whales *B. acutorostrata scammoni*, *M. monoceros*, and *P. macrocephalus*) have prismatic enamel or at least some degree of prism development (Group I, table 1). The animals without prismatic enamel, except the whales, lack a predicted AH in Ambn (Groups IV and V, table 1). The two eutherians (*E. edwardii* and *F. damarensis*) and the four marsupials (*M. domestica*, *S. harrisii*, *D. gliroides*, and *P. cinereus*) do not have a predicted AH motif but have prismatic enamel (Group II, table 1).

The experimental data summarized in table 3 confirmed the presence of the predicted AH motif in Group I, and the presence of the functional but nonpredicted AH motif in Group II. In contrast, those species without prismatic enamel, Groups IV and V, do not have a functional AH, conforming to our predictions. Typically, an

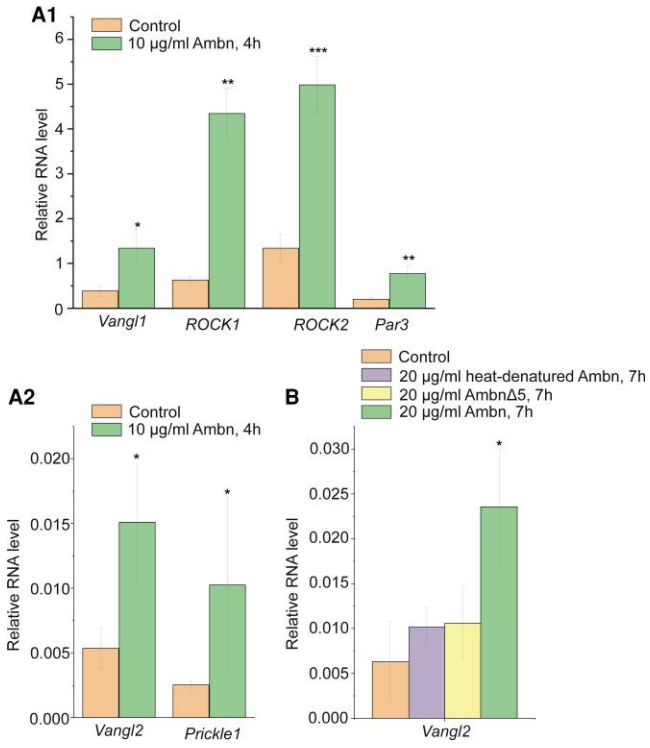

Fig. 7. Expression of *Vangl1*, *ROCK1*, *ROCK2*, *PAR3*, *Vangl2*, and *PRICKLE1* in LS8 cells treated with recombinant Ambn and its variants. *A1*, Relative RNA levels of *VANGL1*, *ROCK1*, *ROCK2*, and *PAR3* in LS8 cells treated with 10 μg/ml Ambn for 4 h. *A2*, Relative RNA levels of *VANGL2* and *PRICKLE1* in LS8 cells treated with 10 μg/ml Ambn for 4 h. *B*, Relative RNA levels of *VANGL2* in LS8 cells treated with 20 μg/ml heat-denatured Ambn (negative control), AmbnΔ5 and Ambn for 7 h. $^{*}P < 0.05$; $^{**}P < 0.01$; $^{***}P < 0.001$.

AH motif interacts with a lipid membrane through three steps: electrostatic attraction, adsorption, and conformational change (Seelig 2004). The experimental data clearly show that the peptides of Group I, which have prismatic enamel, bind to liposomes as shown by intrinsic fluorescence spectra, and then exhibit the typical behavior of an AH, that is, random coil-to-helix transition (Seelig 2004), as shown by CD spectra. These peptides were adsorbed onto liposomes (LUV) and inserted into the bilayer lipid membrane, as shown by membrane leakage assay. They also actively competed with the full-length Ambn coated on a plate to inhibit the spreading of LS8 and ALC cells. These data showed that peptides of Group I have typical AH behaviors and are functional. The peptides derived from *E. edwardii* and *M. domestica* of Group II, both of which come from species that have prismatic enamel, were attracted to liposomes and exhibited a conformational transition evidenced by the decrease of an upward peak at around 222 nm in the CD spectrum. This upward peak was related to protein aggregation (Benjwal et al. 2006), likely because of the high peptide concentration required by the CD experiments and was consistent with the observed turbidity in a cuvette (data not shown). The observation that these peptides inserted into the bilayer lipid membrane (leaked the LUV) and inhibited cell spreading indicated that they form a functional AH, even though the random coil-to-helix transition could not be observed by CD. The peptide from *P. vampyrus* of Group III was attracted by liposomes, underwent slight conformational transition, caused slight liposome leakage, and did not inhibit the spreading of LS8 or ALC cells. *P. vampyrus* lacks an AH, and thus might have poorly prismatic enamel or might even be prismless. In contrast to the peptides of Groups I and II, which have prismatic enamel, the peptides of Group IV and Group V did not form a functional AH, even though the peptides of Group IV could be attracted to liposomes. The three whales in Group VI have an AH motif but these species have no prismatic enamel. This might be because the *B. acutorostrata scammoni* has inactivated *Enam*, *Mmp20*, and *Amel* genes (Yim et al. 2014); *M. monoceros* has a premature stop codon in exon 13 of *Ambn* (Meredith et al. 2013); and *P. macrocephalus* has inactivated *ACP4* (Randall et al. 2021). The correlation between the AH and prismatic structure therefore is not relevant for these three whales.

Interestingly, the peptides of Group II have no predicted AH due to a proline residue in the middle, but the experimental data showed that these peptides form a functional AH. A proline residue in the middle of an amino acid sequence is generally supposed to break α-helical and β-sheet structures in water-soluble proteins because its side chain cyclizes back to the backbone amide, leaving one of its dihedral angles (φ) fixed at ca. −65° (Kumeta et al. 2018; Richardson and Richardson 1988). However, proline is not an intrinsic α -helix breaker when the protein is associated with a membrane (Williamson 1994; Li et al. 1996). Peptides from *E. edwardii* and *M. domestica*, each of which have a proline in the middle of their amino acid sequence, were thus not expected to form helices based on predictions *in silico*. When these peptides were adsorbed onto liposomes, the residues facing the membrane were in a membrane-mimetic environment instead of an aqueous one, which would greatly enhance the

Table 3. Summary of the Biophysical and Cell-based Experiments Demonstrating the Secondary Structural Characteristics of Ambn-derived AH Peptides From Different Species and Their Effects on Cell Spreading.

Group	Species	Fluo	CD	Membrane leakage	LS8	ALC	Enamel microstructure	Predicted AH	Expermental validated AH
I	*Homo sapiens*	+	+	++	+	+	Prismatic	Y	Y
	Mus musculus	+	+	++	++	+	Prismatic	Y	Y
	Ornithorhynchus anatinus	+	+	+	+	+	Prismatic	Y	Y
II	*Elephantulus edwardii*	+	?	+	++	+	Prismatic	N	Y
	Monodelphis domestica	+	?	+	+	+	Prismatic	N	Y
III	*Pteropus vampyrus*	+	?	?	–	–	Poor prismatic[a]	N	N
IV	*Dasypus novemcinctus*	+	?	?	–	–	Prismless	N	N
	Orycteropus afer afer	+	–	?	–	–	Prismless	N	N
V	*Alligator mississippiensis*	–	–	–	–	–	Prismless	N	N
	Xenopus laevis	–	–	–	–	–	Prismless	N	N

In Fluo(rescence) column, "+" indicates a blue shift in the intrinsic fluorescence spectra, suggesting there is a interaction; "–" indicates an absence of blue shift, suggesting there is no interaction. In CD column, "+" indicates a helix is formed in the presence of LUV, "–" indicates no increase in helical content, "?" indicates inconclusive results. In Membrane leakage column, "++" indicates the peptides cause severe LUV leakage, "+" indicates the peptides cause mild leakage, "?" indicates the peptides cause slight leakage and inconclusive results, "–" indicates no leakage. In LS8 and ALC column, "++" indicates the peptides inhibit cell spreading severely, "+" indicates the peptides inhibit cell spreading moderately, "–" indicates no detectable inhibition. In Predicted AH and Experimental validated AH; "Y" indicates a predicted or validated AH, "N" indicates indicates no predicted or validated AH.

[a]Enamel microstructure was inferred from that of other species in the same genus.

helical propensity of proline, and the proline could help to stabilize the α-helical conformation (Williamson 1994; Li et al. 1996). Prolines in α-helices can confer structural flexibility and functional integrity to a protein (Kumeta et al. 2018). Thus, peptides from *E. edwardii* and *M. domestica* could form a functional AH when they were adsorbed onto liposomes. Leakage and cell spreading assays with the peptide of *S. harrisii* (FSRFGFGKQFNPLWMHGLLP) (supplementary fig. S4, Supplementary Material online) further supported this observation. Thus, the two studied eutherians (*E. edwardii* and *F. damarensis*) and four marsupials (*M. domestica*, *S. harrisii*, *D. gliroides*, and *P. cinereus*) have a functional AH with a medial proline.

Our detailed *in silico* sequence analysis together with experimental data using synthetic peptides and liposomes collectively showed that, out of a total of 51 species (excluding *O. hannah and P. bivittatus*), 43 species (86.3% of the total, including 26 from Group I, 6 from Group II, 2 from Group IV, and 9 from Group V) support the correlation between the presence of AH and emergence of prismatic enamel. Four additional species (7.8%) from Group I may support the link, one species (2.0%) from Group III may or may not support it, and three species (5.9%, Group VI, the three whales) are not relevant. Notably, the sequences of the synthetic peptides can in many cases be found in more than just the one representative species listed in table 2. The species with sequences identical to the synthetic peptides derived from AH motifs have prismatic enamel, while the species with sequences identical to the synthetic peptides derived from equivalent regions without AH lack prismatic enamel. Therefore, the correlation between AH and prismatic enamel can be expanded to more than the 53 species analyzed in this study. The observation that an AH motif was found in *O. anatinus* is another strong support that the AH motif coemerged with prismatic enamel. It is noteworthy that one extant reptile, *U. maliensis*, has prismatic or prism-like enamel structures (Diekwisch 2020). However, when examined in detail, the prisms are not like those in mammalian prismatic enamel (Sander 1997; Wood et al. 1999). Because Tomes' processes (or Tomes' process-like structures) are formed in *Uromastyx*, there might be a similar correlation between its prismatic structure, Tomes' process, and an AH motif in some matrix protein of *U. maliensis*.

During enamel formation, ameloblasts retract from the extracellular space within which enamel is formed. Precise and coordinated directional movement of ameloblasts together with extracellular matrix secretion dictate the prismatic architecture of enamel. Tomes' processes of ameloblasts have been associated with the secretion and organization of enamel matrix proteins, the alignment of hydroxyapatite crystallites and ultimately the prismatic patterns of mature enamel (Moss-Salentijn et al. 1997). Ambn was shown to colocalize with the cell membrane at the Tomes' process (Su et al 2020). The novel association between the AH domain in Ambn sequence and enamel prismatic structure in this study is proposed to be related to a few extracellular molecular events involving Ambn protein interacting with different targets. These events include matrix-cell adhesion, control of enamel apatite crystal initiation and growth (Lu et al 2011), as well as formation of enamel prismatic structure. The interacting targets may include other enamel matrix proteins (Su et al. 2016; Bapat et al 2020), the cell surface (via the AH domain) (Su et al 2020), and the mineral (Shao et al 2022). Our present findings suggest that in addition to cell membrane binding and enamel matrix association, Ambn may be involved in signaling pathways related to ameloblast differentiation and/or cell polarization during early stages of enamel development. We speculate that after being anchored to ameloblasts' cell membrane, Ambn might cooperate with other enamel matrix proteins such as amelogenin, enamelin, laminins, and integrins to trigger signaling pathways related to cell movement/polarization and perhaps to regulate the development of Tomes' process (Simmer et al. 2021).

Consistent with the above hypothesis, in a recent study from our laboratory we reported that ameloblastin causes cell elongation and polarization in 3D cultures of ameloblast cell lines (Visakan et al. 2022). Preferential cell elongation was characterized by increased cell aspect ratio, and polarization by the asymmetrical distribution of cell junctional complex and polarity protein markers such as E-cadherin, Par3, and Claudin-1 within the elongated cells. Furthermore, it was observed that the AH-containing Exon 5-encoded region of *Ambn* was largely responsible for these cell effects. Heat-denaturing or deletion of Exon 5 led to the dysfunction of Ambn in promoting gene expression associated to cell polarization. These observations suggested that the AH motif encoded by the sequence in Exon 5 is involved in molecular events to initiate cell polarization or morphological changes. The present RT-PCR data showed that addition of Ambn to ameloblast-like LS8 cells regulates the expression of cell polarization genes including *Vangl2*, *Vangl1*, *Prickle1*, *ROCK1*, and *ROCK2*. Ambn not only influences polarization, differentiation and proliferation of ameloblasts, but it also affects extracellular matrix signaling pathways in cell culture systems. It has been reported that Ambn modulates osteoclastogenesis through the integrin/ERK pathway (Lu et al. 2013), may indirectly suppress RANKL-induced osteoclastogenesis via MAPK signaling pathway (Chaweewannakorn et al. 2017), and may affect cell adhesion via RhoA signaling pathway and cell cycle progression through p27 (Zhang et al. 2011). In the case of enamel, like BAR domain proteins, which also have amphipathic helices (Carman and Dominguez 2018), Ambn may serve as a multi-functional hub that adheres to the cells while initiating signaling pathways, and thus may be involved in the development of Tomes' processes.

In summary, we present a correlation between the emergence of the AH motif of Ambn and the evolution of prismatic enamel in mammals. Our thorough Ambn sequence analysis provides insight into the origin of prismatic enamel, which is one of the central questions in the evolution of ectodermal hard tissues. We speculate that the AH motif evolved to trigger signaling pathways for initiation of cell polarization or morphological changes including Tomes' processes of ameloblasts. Future investigation is needed to explore the mechanism of action of such signaling pathways.

Materials and Methods

Bioinformatic and Molecular Evolution Analysis of Ambn in Relation to Enamel Structure

A total of 53 full-length Ambn protein sequences, representative of major lineages, were extracted from the GenBank or UniProt databases (supplementary table S1, Additional file 1, Supplementary Material online). Enamel microstructures and their references are summarized in supplementary table S2, Additional file 1, Supplementary Material online. Sequence alignment was conducted with Mafft (v7.504) using E-INS-i method which is suitable for sequences with long unalignable regions (Katoh et al. 2005). The time-tree was generated using the RelTime method. Divergence times for all branching points in the topology were calculated using the Maximum Likelihood method and JTT matrix-based model (Jones et al. 1992). The estimated log likelihood value of the topology shown is −12469.17. A discrete Gamma distribution was used to model evolutionary rate differences among sites (five categories [+G, parameter = 2.5577]). The tree is drawn to scale, with branch lengths measured in the relative number of substitutions per site. All positions with less than 95% site coverage were eliminated, that is, fewer than 5% alignment gaps, missing data, and ambiguous bases were allowed at any position (partial deletion option). There was a total of 298 positions in the final dataset. Evolutionary analyses were conducted in MEGA11 (Tamura et al. 2021), and the number of bootstrap replications was 1000. *Lepisosteus oculatus* was selected as an outgroup species because it is a species of ray-finned bony fish, which do not share the common ancestor of tetrapods (Braasch et al. 2016). The bootstrap probability (Pb) of 32 interior branches of the tree was higher than 70; Pb of 11 interior branches was higher than 50; and Pb of 7 interior branches was less than 50.

The projection of Ambn protein sequences in a helical wheel (fig. 2) was calculated by Heliquest service at http://heliquest.ipmc.cnrs.fr/(Gautier et al. 2008). Hydrophobic moment (<μH>) and net charge (z) of every 18 residues were applied to calculate the discriminant factor (D factor) by the following equation: $D = 0.944(<\mu H>) + 0.33\ (z)$ (https://heliquest.ipmc.cnrs.fr/HelpProcedure.htm#heading2). If the *D* factor is smaller than 0.68, the sequence is assigned to be "not an AH". If the *D* factor is greater than 1.34 and there is a hydrophobic surface, the sequence is assigned to be "an AH". If the *D* factor is between 0.68 and 1.34 and there is a hydrophobic surface, the sequence may be "an AH". If there is a proline residue in the middle, the sequence was assumed to be "not an AH" before being validated by experimental data.

Protein Expression and Purification

Recombinant mouse ameloblastin (rAmbn) and the variant delta 5 (AmbnΔ5), which lacks the sequence encoded by Exon 5, were expressed and purified following the method described in our recent publication (Su et al. 2019b). Briefly, Ambn was expressed in *Escherichia coli* with Histidine (His), Thioredoxin (Trx), and S-tags in BL21, using pET-32a plasmid (Novagen) with inserted mouse *Ambn* gene (GenBank No. AAB93765.1). The expressed protein was purified using Nickel affinity chromatography (Ni-NTA Agarose, Qiagen), followed by dialysis through 10K MWCO dialysis membrane (SnakeSkin™ Dialysis Tubing, ThermoFisher). His-, Trx-, and S-tags were cleaved by Enterokinase (light chain, New England Biolabs), and were removed by a reversed phase High Performance Liquid Chromatography (HPLC) system (Varian Prostar system with Agilent OpenLab CDS software). Phenomenex C4 column (10 × 250 mm, 5 μm) was used, and proteins were

eluted with an increasing gradient of 32–72% acetonitrile over 80 min, at a flow rate of 1.5 ml/min. Collected proteins were lyophilized and characterized with SDS-PAGE. The heat denaturation of rAmbn was performed by heating rAmbn at 95°C for 10 min.

Peptide Synthesis

The peptides were designed based on the potential amphipathic helices in Ambn, and were synthesized by Biomer Technology (CA, USA) with a purity of 95%. The rational for the design and details of their sequences are listed in tables 1 and 2.

Unilamellar Lipid Vesicle Preparation

LUVs, mimicking the membrane domain involved in epithelial cell–ECM adhesion (Márquez et al. 2008), were prepared in pH 7.4 buffer containing 10.0 mM HEPES, 50.0 mM KCl, 1.0 mM EDTA, and 3.0 mM NaN_3, as previously described (Su et al. 2019). The lipid composition was with a lipid molar ratio of 1-palmitoyl-2-oleoyl-sn-glycero-3-phosphocholine (POPC): 1-palmitoyl-2-oleoyl-sn-glycero-3-phosphoethanolamine (POPE): 1-palmitoyl-2-oleoyl-sn-glycero-3-phospho-L-serine (POPS): 1-palmitoyl-2-oleoyl-sn-glycero-3-phosphoinositol(POPI) : sphingomyelin (SM) = 40:25:15:10:10 (Avanti Polar Lipids). Note that POPC, POPE, and SM have neutral charge, while POPS and POPI are negatively charged. Therefore, the ECM-adhesion-imitating LUVs used here are about 25% anionic. The size of the LUVs was 400 nm.

Intrinsic Tryptophan Fluorescence Spectroscopy

100 μM peptides were prepared in pH 7.4, 10.0 mM Tris–HCl buffer, and kept at 4°C overnight. The peptides were diluted to 10 μM in pH 7.4, 10.0 mM Tris–HCl buffer, and then mixed with 300 μM, 100 nm LUVs and kept at room temperature for 5.0 min before measurements. Tryptophan fluorescence spectra were recorded on a Quanta Master 4 fluorescence spectro-fluorometer (HORIBA Scientific). The excitation wavelength was 295 nm, the emission wavelength range was 300–400 nm, and all the split widths were 5 nm.

CD Spectroscopy

100 μM peptides were prepared in pH 7.4, 10.0 mM Tris–HCl buffer, and kept at 4°C overnight. Then, 100 μM peptides were mixed with 300 μM, 100 nm LUVs in pH 7.4, 10.0 mM Tris–HCl buffer and kept at room temperature for 5.0 min before measurements. Far-UV CD spectra were recorded on a J-815 circular dichroism spectrometer (JASCO) over a wavelength range of 190–260 nm using a 1 mm path length quartz cell.

Membrane Leakage Assay

For membrane leakage assays, 400 nm LUVs were prepared encapsulating 9.0 mM ANTS (8-aminonaphthalene-1,3,6-trisulfonic acid) and 25.0 mM DPX (p-xylene-bis-pyridinium bromide), following previous methods (Su et al. 2019a). 300 μM 100 nm LUVs encapsulating 9.0 mM ANTS and 25.0 mM DPX were mixed separately with 1 μM peptides. 0.05% Triton X-100 were used as controls. Release of fluorophore ANTS was monitored by measuring the increase of ANTS fluorescence intensity using a Quanta Master 4 fluorescence spectro-fluorometer (HORIBA Scientific). Excitation and emission wavelengths were 380 and 520 nm. All data were normalized to the fluorescence intensity when all the vesicles were disrupted by Triton X-100.

Cell Spreading Assay

Cell spreading assays were conducted following published protocols (Humphries 2001; Sonoda et al. 2009). LS8 (Chen et al. 1992) and ALC cells (Nakata et al. 2003) representing different stages of ameloblast cells were cultured in low glucose Dulbecco's modified Eagle's Medium (DMEM) (Corning) containing 100 U/L penicillin and 100 mg/ml streptomycin and 10% heat-inactivated fetal bovine serum (Corning) in a 5.0% CO_2 atmosphere at 37°C. The assay was performed in 96-well cell culture plates (Cellstar), which were coated with 100 μl 5 μg/ml recombinant mouse Ambn in pH 7.4 PBS, and then were blocked with 50 μl 10 mg/ml BSA in in divalent cation-free PBS for 1–2 h at room temperature. The cells were treated with peptides. For a single well, about 1.0×10^4 cells were added. After incubation for 2 h for LS8 cells or 1.5 h for ALC cells, the percentage of cells that adopted spread morphology was determined using a microscope.

RT-PCR

Confluent LS8 cells in a 12-well plate were treated with 10 μg/ml Ambn for 4 h, or with 20 μg/ml Ambn, heat-denatured Ambn, or AmbnΔ5 for 7 h. After treatment, the RNA was purified by RNeasy Plus Mini Kit (Qiagen) following the kit's instructions. Then, reverse transcription of RNA into cDNA was conducted using iScript Reverse Transcription Supermix for RT-qPCR (Bio-rad). Finally, the relative RNA levels of *Vangl1*, *Vangl2*, *ROCK1*, *ROCK2*, *Par3*, and *Prickle1* were detected by CFX96 Real-Time System (Bio-rad) using iQ SYBR Green Supermix and the primers listed in supplementary table S3, Supplementary Material online.

Statistical Analysis

Statistical analysis was carried out using one-tailed Student's *t*-tests in Microsoft Excel. The differences were considered significant if $P < 0.05$. All data were representative of at least three independent experiments using different batches of purified proteins.

Supplementary Material

Supplementary data are available at *Molecular Biology and Evolution* online.

Acknowledgments

This project was funded by the National Institutes of Health–National Institute of Dental and Craniofacial

Research grants DE-027632 and DE-013414 to J.M.-O. R90 fellowship DE022528 to Dr M.L. Paine supported R.A.B. We thank Dr Malcolm Snead for providing LS8 cells, Dr Toshihiro Sugiyama for providing ALC cells, Dr Shuxing Li (NanoBiophysics Center, USC) for assistance with CD and fluorescence spectra, and Dr Bridget Samuels for proofreading and editing the manuscript.

Author Contributions

J.S. and J.M.-O. contributed to conception, design, data acquisition, analysis, and interpretation, drafted and critically revised the manuscript; R.A.B. and G.V. contributed to data acquisition and analysis, critically revised the manuscript. All authors gave final approval and agreed to be accountable for all aspects of the work.

Data Availability Statement

The data underlying this article are available in the article and in its online supplementary material.

Conflict of Interest Statement

The authors declare no potential conflicts of interest with respect to the authorship and/or publication of this article.

References

Al-Hashimi N, Sire JY, Delgado S. 2009. Evolutionary analysis of mammalian enamelin, the largest enamel protein, supports a crucial role for the 32-kDa peptide and reveals selective adaptation in rodents and primates. *J Mol Evol*. **69**:635–656.

Alloing-Séguier L, Marivaux L, Barczi J-F, Lihoreau F, Martinand-Mari C. 2019. Relationships between enamel prism decussation and organization of the ameloblast layer in rodent incisors. *Anat Rec*. **302**:1195–1209.

Bapat RA, Su J, Moradian-Oldak J. 2020. Co-Immunoprecipitation reveals interactions between amelogenin and ameloblastin via their self-assembly domains. *Front Physiol*. **11**:622086.

Benjwal S, Verma S, Röhm K-H, Gursky O. 2006. Monitoring protein aggregation during thermal unfolding in circular dichroism experiments. *Protein Sci*. **15**:635–639.

Berkovitz B, Shellis P. 2017. Enameloid and enamel. In: Berkovitz B, Shellis P, editors. *The teeth of non-mammalian vertebrates*. Amsterdam, Netherlands: Academic Press. p. 311–330.

Beyeler M, Schild C, Lutz R, Chiquet M, Trueb B. 2010. Identification of a fibronectin interaction site in the extracellular matrix protein ameloblastin. *Exp Cell Res*. **316**:1202–1212.

Boyde A. 1997. Microstructure of enamel. In: Chadwick DJ and Cardew G, editors. *Ciba foundation symposium 205—dental enamel*. Chichester: John Wiley & Sons. p. 18–31.

Boyde A, Martin L. 1984. The microstructure of primate dental enamel. In: Chivers DJ Wood BA and Bilsborough A, editors. *Food acquisition and processing in primates*. Boston, MA: Springer US. p. 341–367.

Braasch I, Gehrke AR, Smith JJ, Kawasaki K, Manousaki T, Pasquier J, Amores A, Desvignes T, Batzel P, Catchen J, *et al.* 2016. The spotted gar genome illuminates vertebrate evolution and facilitates human-teleost comparisons. *Nat Genet*. **48**:427–437.

Brady JP, Claridge JK, Smith PG, Schnell JR. 2015. A conserved amphipathic helix is required for membrane tubule formation by Yop1p. *Proc Natl Acad Sci U S A*. **112**:E639–E648.

Carman PJ, Dominguez R. 2018. BAR Domain proteins—a linkage between cellular membranes, signaling pathways, and the actin cytoskeleton. *Biophys Rev*. **10**:1587–1604.

Cerny R, Slaby I, Hammarstrom L, Wurtz T. 1996. A novel gene expressed in rat ameloblasts codes for proteins with cell binding domains. *J Bone Miner Res*. **11**:883–891.

Chaweewannakorn W, Ariyoshi W, Okinaga T, Morikawa K, Saeki K, Maki K, Nishihara T. 2017. Ameloblastin and enamelin prevent osteoclast formation by suppressing RANKL expression via MAPK signaling pathway. *Biochem Biophys Res Commun*. **485**:621–626.

Chen LS, Couwenhoven RI, Hsu D, Luo W, Snead ML. 1992. Maintenance of amelogenin gene expression by transformed epithelial cells of mouse enamel organ. *Arch Oral Biol*. **37**:771–778.

Chiba Y, Yoshizaki K, Saito K, Ikeuchi T, Iwamoto T, Rhodes C, Nakamura T, de Vega S, Morell RJ, Boger ET, *et al.* 2020. G protein-coupled receptor Gpr115 (Adgrf4) is required for enamel mineralization mediated by ameloblasts. *J Biol Chem*. **295**:15328–15341.

Cui FZ, Ge J. 2007. New observations of the hierarchical structure of human enamel, from nanoscale to microscale. *J Tissue Eng Regen Med*. **1**:185–191.

Davit-Béal T, Chisaka H, Delgado S, Sire J-Y. 2007. Amphibian teeth: current knowledge, unanswered questions, and some directions for future research. *Biol Rev*. **82**:49–81.

Davit-Béal T, Tucker AS, Sire J-Y. 2009. Loss of teeth and enamel in tetrapods: fossil record, genetic data and morphological adaptations. *J Anat*. **214**:477–501.

Delgado S, Girondot M, Sire J-Y. 2005. Molecular evolution of amelogenin in mammals. *J Mol Evol*. **60**:12–30.

Delsuc F, Gasse B, Sire JY. 2015. Evolutionary analysis of selective constraints identifies ameloblastin (AMBN) as a potential candidate for amelogenesis imperfecta. *BMC Evol Biol*. **15**:148.

Diekwisch TGH. 2020. Evolution: herbivore-type teeth in a cretaceous tuatara relative. *Curr Biol*. **30**:R395–R397.

Diekwisch TG, Jin T, Wang X, Ito Y, Schmidt M, Druzinsky R, Yamane A, Luan X. 2009. Amelogenin evolution and tetrapod enamel structure. *Front Oral Biol*. **13**:74–79.

Du C, Falini G, Fermani S, Abbott C, Moradian-Oldak J. 2005. Supramolecular assembly of amelogenin nanospheres into birefringent microribbons. *Science*. **307**:1450–1454.

Fang PA, Conway JF, Margolis HC, Simmer JP, Beniash E. 2011. Hierarchical self-assembly of amelogenin and the regulation of biomineralization at the nanoscale. *Proc Natl Acad Sci U S A*. **108**:14097–14102.

Fincham AG, Moradian-Oldak J, Diekwisch TG, Lyaruu DM, Wright JT, Bringas P Jr., Slavkin HC. 1995. Evidence for amelogenin "nanospheres" as functional components of secretory-stage enamel matrix. *J Struct Biol*. **115**:50–59.

Fukumoto S, Kiba T, Hall B, Iehara N, Nakamura T, Longenecker G, Krebsbach PH, Nanci A, Kulkarni AB, Yamada Y. 2004. Ameloblastin is a cell adhesion molecule required for maintaining the differentiation state of ameloblasts. *J Cell Biol*. **167**:973–983.

Gasse B, Chiari Y, Silvent J, Davit-Béal T, Sire J-Y. 2015. Amelotin: an enamel matrix protein that experienced distinct evolutionary histories in amphibians, sauropsids and mammals. *BMC Evol Biol*. **15**:47.

Gautier R, Douguet D, Antonny B, Drin G. 2008. HELIQUEST: a web server to screen sequences with specific alpha-helical properties. *Bioinformatics*. **24**:2101–2102.

Giménez-Andrés M, Čopič A, Antonny B. 2018. The many faces of amphipathic helices. *Biomolecules*. **8**:45.

Hatzakis NS, Bhatia VK, Larsen J, Madsen KL, Bolinger P-Y, Kunding AH, Castillo J, Gether U, Hedegård P, Stamou D. 2009. How curved membranes recruit amphipathic helices and protein anchoring motifs. *Nat Chem Biol*. **5**:835–841.

Hu J-C, Chun Y-H, Al Hazzazzi T, Simmer JP. 2007. Enamel formation and amelogenesis imperfecta. *Cells Tissues Organs*. **186**:78–85.

Hu J-C, Hu Y, Lu Y, Smith CE, Lertlam R, Wright JT, Suggs C, McKee MD, Beniash E, Kabir ME, *et al.* 2014. Enamelin is critical for ameloblast integrity and enamel ultrastructure formation. *PLoS One*. **9**:e89303.

Humphries MJ. 2001. Cell adhesion assays. *Mol Biotechnol*. **18**:57–61.

Iizuka S, Kudo Y, Yoshida M, Tsunematsu T, Yoshiko Y, Uchida T, Ogawa I, Miyauchi M, Takata T. 2011. Ameloblastin regulates osteogenic differentiation by inhibiting Src kinase via cross talk between integrin beta1 and CD63. *Mol Cell Biol*. **31**:783–792.

Jin T, Ito Y, Luan X, Dangaria S, Walker C, Allen M, Kulkarni A, Gibson C, Braatz R, Liao X, *et al.* 2009. Elongated polyproline motifs facilitate enamel evolution through matrix subunit compaction. *PLoS Biol*. **7**:e1000262.

Jones DT, Taylor WR, Thornton JM. 1992. The rapid generation of mutation data matrices from protein sequences. *Bioinformatics*. **8**: 275–282.

Katoh K, Kuma K-I, Toh H, Miyata T. 2005. MAFFT Version 5: improvement in accuracy of multiple sequence alignment. *Nucleic Acids Res*. **33**:511–518.

Kawasaki K, Amemiya CT. 2014. SCPP Genes in the coelacanth: tissue mineralization genes shared by sarcopterygians. *J Exp Zool B Mol Dev Evol*. **322**:390–402.

Kawasaki K, Suzuki T. 2011. Molecular evolution of matrix metalloproteinase 20. *Eur J Oral Sci*. **119**:247–253.

Kawasaki K, Weiss KM. 2008. SCPP Gene evolution and the dental mineralization continuum. *J Dent Res*. **87**:520–531.

Krebsbach PH, Lee SK, Matsuki Y, Kozak CA, Yamada KM, Yamada Y. 1996. Full-length sequence, localization, and chromosomal mapping of ameloblastin a novel tooth-specific gene. *J Biol Chem*. **271**:4431–4435.

Kumeta M, Konishi HA, Zhang W, Sakagami S, Yoshimura SH. 2018. Prolines in the α-helix confer the structural flexibility and functional integrity of importin-β. *J Cell Sci*. **131**:jcs206326.

Lacruz RS, Nakayama Y, Holcroft J, Nguyen V, Somogyi-Ganss E, Snead ML, White SN, Paine ML, Ganss B. 2012. Targeted overexpression of amelotin disrupts the microstructure of dental enamel. *PLoS One*. **7**:e35200.

Lester KS, Boyde A. 1986. Scanning microsc of platypus teeth. *Anat Embryol*. **174**:15–26.

Lester KS, Boyde A, Gilkeson C, Archer M. 1987. Marsupial and monotreme enamel structure. *Scanning microsc*. **1**:401–420.

Lester K, Hand S. 1986. Chiropteran enamel structure. *Scanning microsc*. **1**:37.

Lester K, Von Koenigswald W. 1989. Crystallite orientation discontinuities and the evolution of mammalian enamel–or, when is a prism? *Scanning microsc*. **3**:28.

Li S-C, Goto NK, Williams KA, Deber CM. 1996. Alpha-helical, but not beta-sheet, propensity of proline is determined by peptide environment. *Proc Natl Acad Sci*. **93**:6676–6681.

Liang T, Hu Y, Smith CE, Richardson AS, Zhang H, Yang J, Lin B, Wang S-K, Kim J-W, Chun Y-H, *et al.* 2019. AMBN Mutations causing hypoplastic amelogenesis imperfecta and ambn knockout-NLS-lacZ knockin mice exhibiting failed amelogenesis and ambn tissue-specificity. *Mol Genet Genomic Med*. **7**:e929.

Line SRP, Novaes PD. 2005. The development and evolution of mammalian enamel: structural and functional aspects. *Braz J Morphol Sci*. **22**:67–72.

Loch C, Duncan W, Simões-Lopes PC, Kieser JA, Fordyce RE. 2013. Ultrastructure of enamel and dentine in extant dolphins (cetacea: delphinoidea and inioidea). *Zoomorphology* **132**: 215–225.

Lu X, Ito Y, Atsawasuwan P, Dangaria S, Yan X, Wu T, Evans CA, Luan X. 2013. Ameloblastin modulates osteoclastogenesis through the integrin/ERK pathway. *Bone*. **54**:157–168.

Lu X, Ito Y, Kulkarni A, Gibson C, Luan X, Diekwisch TG. 2011. Ameloblastin-rich enamel matrix favors short and randomly oriented apatite crystals. *Eur J Oral Sci*. **119**(Suppl 1):254–260.

Márquez MG, Nieto FL, Fernández-Tome MC, Favale NO, Sterin-Speziale N. 2008. Membrane lipid composition plays a central role in the maintenance of epithelial cell adhesion to the extracellular matrix. *Lipids*. **43**:343–352.

Mazumder P, Prajapati S, Bapat R, Moradian-Oldak J. 2016. Amelogenin-ameloblastin spatial interaction around maturing enamel rods. *J Dent Res*. **95**:1042–1048.

Meredith RW, Gatesy J, Springer MS. 2013. Molecular decay of enamel matrix protein genes in turtles and other edentulous amniotes. *BMC Evol Biol*. **13**:20.

Messer M, Weiss AS, Shaw DC, Westerman M. (Messer1998 coauthors). 1998. Evolution of the monotremes: phylogenetic relationship to marsupials and eutherians, and estimation of divergence dates based on α-lactalbumin amino acid sequences. *J Mamm Evol*. **5**:95–105.

Moradian-Oldak J. 2012. Protein-mediated enamel mineralization. *Front Biosci*. **17**:1996.

Moss-Salentijn L, Moss ML, Yuan MS-T. 1997. The ontogeny of mammalian enamel. In: Wighart v. Koenigswald and Martin Sander P, editors. *Tooth enamel microstructure*: London: CRC Press. p. 5–30.

Nakata A, Kameda T, Nagai H, Ikegami K, Duan Y, Terada K, Sugiyama T. 2003. Establishment and characterization of a spontaneously immortalized mouse ameloblast-lineage cell line. *Biochem Biophys Res Commun*. **308**:834–839.

Nanci A, Warshawsky H. 1984. Relationship between the quality of fixation and the presence of stippled material in newly formed enamel of the rat incisor. *Anat Rec*. **208**:15–31.

Nishikawa S, Kawamoto T. 2015. Localization of core planar cell polarity proteins, PRICKLEs, in ameloblasts of rat incisors: possible regulation of enamel rod decussation. *Acta Histochem Cytochem* **48**:37–45.

Nuin PAS, Wang Z, Tillier ERM. 2006. The accuracy of several multiple sequence alignment programs for proteins. *BMC Bioinf*. **7**: 471.

Otsu K, Harada H. 2016. Rho GTPases in ameloblast differentiation. *Jpn Dent Sci Rev*. **52**:32–40.

Ozdemir D, Hart P, Firatli E, Aren G, Ryu O, Hart T. 2005. Phenotype of ENAM mutations is dosage-dependent. *J Dent Res*. **84**: 1036–1041.

Paine ML, Wang HJ, Luo W, Krebsbach PH, Snead ML. 2003. A transgenic animal model resembling amelogenesis imperfecta related to ameloblastin overexpression. *J Biol Chem*. **278**:19447–19452.

Pataki CI, Rodrigues J, Zhang L, Qian J, Efron B, Hastie T, Elias JE, Levitt M, Kopito RR. 2018. Proteomic analysis of monolayer-integrated proteins on lipid droplets identifies amphipathic interfacial α-helical membrane anchors. *Proc Natl Acad Sci*. **115**: E8172–E8180.

Poulter JA, Murillo G, Brookes SJ, Smith CE, Parry DA, Silva S, Kirkham J, Inglehearn CF, Mighell AJ. 2014. Deletion of ameloblastin exon 6 is associated with amelogenesis imperfecta. *Hum Mol Genet*. **23**:5317–5324.

Qu Q, Haitina T, Zhu M, Ahlberg PE. 2015. New genomic and fossil data illuminate the origin of enamel. *Nature*. **526**:108–111.

Randall JG, Gatesy J, Springer MS. 2021. Molecular evolutionary analyses of tooth genes support sequential loss of enamel and teeth in baleen whales (Mysticeti). *bioRxiv*:2021.2011.2010.468114.

Rensberger JM. 1997. Mechanical adaptation in enamel. In: Wighart v. Koenigswald and Martin Sander P, editors. *Tooth enamel microstructure*. London: CRC Press. p. 237–257.

Rensberger JM, Wang X. 2005. Microstructural reinforcement in the canine enamel of the hyaenid *Crocuta crocuta*, the felidpuma concolorand the late miocene canid borophagus secundus. *J Mamm Evol*. **12**:379–403.

Richardson JS, Richardson DC. 1988. Amino acid preferences for specific locations at the ends of alpha helices. *Science*. **240**:1648.

Sander PM. 1997. Non-mammalian synapsid enamel and the origin of mammalian enamel prisms: the bottom-up perspective. In: Mark F. Teaford MMS, Mark W. J. Ferguson, editor. *Tooth enamel microstructure*. Cambridge: Cambridge University Press. p. 41–62.

Sander PM. 1999. *The microstructure of reptilian tooth enamel: terminology, function, and phylogeny*. München: Verlag Dr. Friedrich Pfeil **38**.

Sander PM. 2000. Prismless enamel in amniotes: terminology, function, and evolution. In: Mark F. Teaford MMS, Mark W. J. Ferguson, editor. *Development, function and evolution of teeth*. Cambridge: Cambridge University Press. p. 92–106.

Sarkar J, Simanian EJ, Tuggy SY, Bartlett JD, Snead ML, Sugiyama T, Paine ML. 2014. Comparison of two mouse ameloblast-like cell lines for enamel-specific gene expression. *Front Physiol*. **5**:277.

Satchell PG, Shuler CF, Diekwisch TGH. 2000. True enamel covering in teeth of the Australian lungfish neoceratodus forsteri. *Cell Tissue Res*. **299**:27–37.

Scholtz JM, Baldwin RL. 1992. The mechanism of alpha-Helix formation by peptides. *Annu Rev Biophys Biomol Struct*. **21**:95–118.

Seelig J. 2004. Thermodynamics of lipid–peptide interactions. *Biochim Biophys Acta Biomembr* **1666**:40–50.

Segrest JP, Garber DW, Brouillette CG, Harvey SC, Anantharamaiah GM. 1994. The amphipathic α helix: a multifunctional structural motif in plasma apolipoproteins. In: Anfinsen CB Edsall JT Richards FM and Eisenberg DS, editors. *Advances in protein chemistry*. New York: Academic Press. p. 303–369.

Shao C, Bapat RA, Su J, Moradian-Oldak J. 2022. Regulation of hydroxyapatite nucleation in vitro through ameloblastin–amelogenin interactions. *ACS Biomater Sci Eng*.

Simmer JP, Hu JCC, Hu Y, Zhang S, Liang T, Wang S-K, Kim J-W, Yamakoshi Y, Chun Y-H, Bartlett JD, *et al*. 2021. A genetic model for the secretory stage of dental enamel formation. *J Struct Biol*. **213**:107805.

Sire JY, Davit-Béal T, Delgado S, Gu X. 2007. The origin and evolution of enamel mineralization genes. *Cells Tissues Organs*. **186**(1): 25–48.

Sire J-Y, Donoghue PCJ, Vickaryous MK. 2009. Origin and evolution of the integumentary skeleton in non-tetrapod vertebrates. *J Anat*. **214**:409–440.

Smith MM. 1978. Enamel in the oral teeth of latimeria chalumnae (pisces: actinistia): a scanning electron microscope study. *J Zool*. **185**:355–369.

Smith CE, Murillo G, Brookes SJ, Poulter JA, Silva S, Kirkham J, Inglehearn CF, Mighell AJ. 2016. Deletion of amelotin exons 3–6 is associated with amelogenesis imperfecta. *Hum Mol Genet*. **25**:3578–3587.

Sonoda A, Iwamoto T, Nakamura T, Fukumoto E, Yoshizaki K, Yamada A, Arakaki M, Harada H, Nonaka K, Nakamura S, *et al*. 2009. Critical role of heparin binding domains of ameloblastin for dental epithelium cell adhesion and ameloblastoma proliferation. *J Biol Chem*. **284**:27176–27184.

Spears IR, Van Noort R, Crompton RH, Cardew GE, Howard IC. 1993. The effects of enamel anisotropy on the distribution of stress in a tooth. *J Dent Res*. **72**:1526–1531.

Su J, Bapat RA, Moradian-Oldak J. 2019b. The expression and purification of recombinant mouse ameloblastin in E. coli. *Methods Mol Biol*. **1922**:229–236.

Su J, Bapat RA, Visakan G, Moradian-Oldak J. 2020. An evolutionarily conserved helix mediates ameloblastin-cell interaction. *J Dent Res*. **99**:1072–1081.

Su J, Chandrababu KB, Moradian-Oldak J. 2016. Ameloblastin peptide encoded by exon 5 interacts with amelogenin N-terminus. *Biochem Biophys Rep*. **7**:26–32.

Su J, Kegulian NC, Bapat RA, Moradian-Oldak J. 2019a. Ameloblastin binds to phospholipid bilayers via a helix-forming motif within the sequence encoded by exon 5. *ACS Omega*. **4**:4405–4416.

Tabuce R, Seiffert ER, Gheerbrant E, Alloing-Séguier L, von Koenigswald W, (Tabuce2017 co-authors). 2017. Tooth enamel microstructure of living and extinct hyracoids reveals unique enamel types among mammals. *J Mamm Evol* **24**:91–110.

Tamura K, Stecher G, Kumar S. 2021. MEGA11: molecular evolutionary genetics analysis version 11. *Mol Biol Evol*. **38**:3022–3027.

Visakan G, Su J, Moradian-Oldak J. 2022. Ameloblastin promotes polarization of ameloblast cell lines in a 3-D cell culture system. *Matrix Biol*. **105**:72–86.

von Koenigswald W. 1985. *Evolutionary trends in the enamel of rodent incisors*. Boston, MA: Springer US. p. 403–422.

Wald T, Spoutil F, Osickova A, Prochazkova M, Benada O, Kasparek P, Bumba L, Klein OD, Sedlacek R, Sebo P, *et al*. 2017. Intrinsically disordered proteins drive enamel formation via an evolutionarily conserved self-assembly motif. *Proc Natl Acad Sci U S A*. **114**: E1641–E1650.

Warren WC, Hillier LW, Marshall Graves JA, Birney E, Ponting CP, Grützner F, Belov K, Miller W, Clarke L, Chinwalla AT, *et al*. 2008. Genome analysis of the platypus reveals unique signatures of evolution. *Nature*. **453**:175–183.

Williamson MP. 1994. The structure and function of proline-rich regions in proteins. *Biochem*. **297**(Pt 2):249–260.

Wood CB, Dumont ER, Crompton AW. 1999. New studies of enamel microstructure in mesozoic mammals: a review of enamel prisms as a mammalian synapomorphy. *J Mamm Evol*. **6**:177–213.

Yamakoshi Y, Tanabe T, Oida S, Hu CC, Simmer JP, Fukae M. 2001. Calcium binding of enamel proteins and their derivatives with emphasis on the calcium-binding domain of porcine sheathlin. *Arch Oral Biol*. **46**:1005–1014.

Yim HS, Cho YS, Guang X, Kang SG, Jeong JY, Cha SS, Oh HM, Lee JH, Yang EC, Kwon KK, *et al*. 2014. Minke whale genome and aquatic adaptation in cetaceans. *Nat Genet*. **46**:88–92.

Young WG, McGowan M, Daley TJ. 1987. Tooth enamel structure in the koala, *Phascolarctos cinereus*: some functional interpretations. *Scanning microsc*. **1**:40.

Zhang Y, Zhang X, Lu X, Atsawasuwan P, Luan X. 2011. Ameloblastin regulates cell attachment and proliferation through RhoA and p27. *Eur J Oral Sci*. **119**(Suppl 1):280–285.